Check for updates

Review

I·M3
Institute of Materials, Minerals & Mining

Science and Technology of Welding and Joining
2024, Vol. 29(2) 99–115
© The Author(s) 2024
Article reuse guidelines:
sagepub.com/journals-permissions
DOI: 10.1177/13621718241235471
journals.sagepub.com/home/stw
Sage

Additive manufacturing of refractory metals and carbides for extreme environments: an overview

Poulomi Mukherjee[1,2], Ashlee Gabourel[1,2], Samad A. Firdosy[3], Douglas C. Hofmann[3] and Atieh Moridi[2]

Abstract

Refractory metals and their carbides possess extraordinary properties when subjected to high temperatures and extreme environments. Consequently, they can act as key material systems for advancing many sectors, including space, energy and defence. However, it has been difficult to process these materials using the conventional routes of manufacturing. Additive manufacturing (AM) has shown a lot of potential to overcome the challenges and develop new material systems with tailored properties. This review provides a fundamental understanding of the challenges in the processing of refractory metals and their carbides, including microcracking, formation of brittle oxide phases and high ductile to brittle transition temperature (DBTT). We also highlight some of the novel approaches that have been taken to improve the processability of these challenging material systems using AM. These include in-situ reactive printing, ultrasonic vibration, laser beam shaping, multi-laser deposition and substrate pre-heating with a focus on microstructural changes to improve the properties of printed parts.

Keywords

high-temperature materials, additive manufacturing, refractory metals, refractory carbides, substrate heating, in-situ synthesis, laser beam shaping, ultrasonic vibration

Received: 5 May 2023; accepted: 4 February 2024

Introduction

Refractory metals and carbides are a class of materials known for their exceptional performance under extreme conditions, making them useful in a wide range of high-temperature and harsh environments. These refractory metals (W, Mo, Nb, Ta, Re, Hf) and their carbides possess outstanding thermal stability, corrosion resistance, wear resistance and remarkable mechanical strength at elevated temperatures.[1–8] In the aerospace and space exploration sectors, refractory metals and carbides are essential for the fabrication of components subjected to the extreme temperatures and stresses encountered during re-entry, rocket propulsion, and space exploration missions. Additionally, they find crucial roles in energy production, particularly in nuclear reactors and gas turbine engines, where their ability to withstand extreme heat and aggressive chemical environments ensures reliable and safe operation.

The production of refractory metals and carbides presents distinctive challenges due to their exceptionally high melting temperatures above 2500 °C. In conventional manufacturing methods, the high processing temperatures are difficult to obtain which results in improper melting, not achieving the desired properties. Additionally, their extreme hardness poses an enduring challenge in terms of tool wear during manufacturing, impacting both process efficiency and cost-effectiveness.[9,10] These materials are often manufactured using casting or powder metallurgical routes.[11–13]

The emergence of additive manufacturing (AM) represents a novel frontier to manufacture ultra-high-temperature refractories and composite structures with favourable microstructures and complex, near-net geometries. For metal matrix composites (MMCs) in particular, in-situ reactions during AM can potentially improve the reinforcement-

[1]Materials Science and Engineering Department, Cornell University, Ithaca, NY, USA
[2]Sibley School of Mechanical and Aerospace Engineering, Cornell University, Ithaca, NY, USA
[3]Jet Propulsion Laboratory, California Institute of Technology, Pasadena, CA, USA

Corresponding author:
Atieh Moridi, Sibley School of Mechanical and Aerospace Engineering, Cornell University, Ithaca, NY, USA.
Email: moridi@cornell.edu

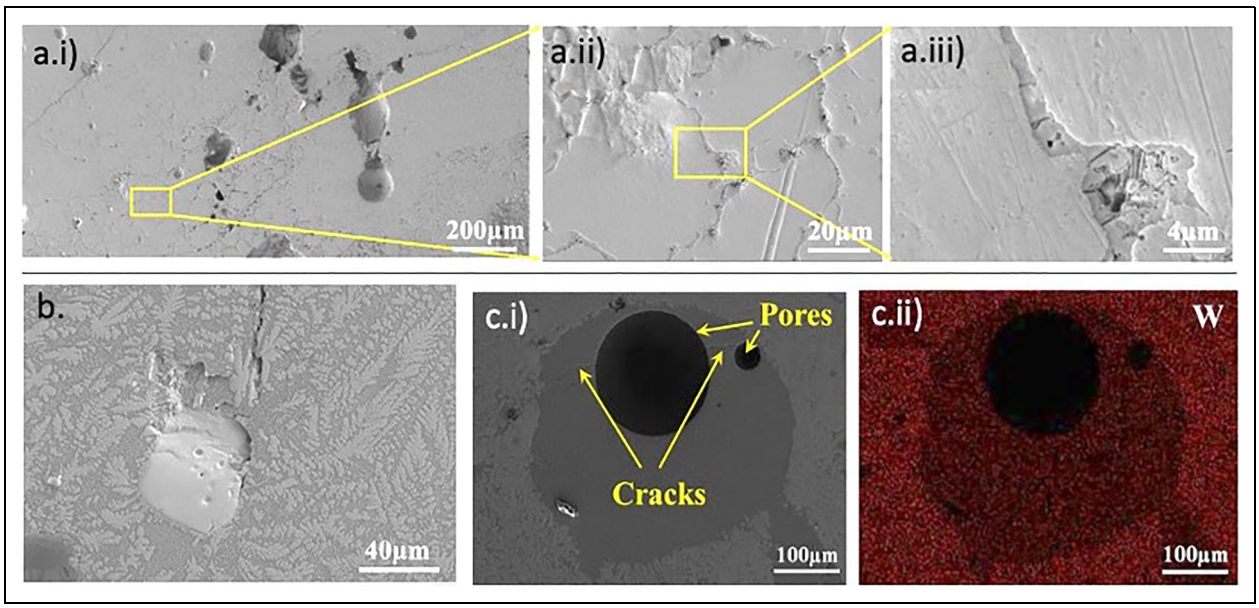

Figure 1. Challenges in processing refractory metal W: (a.i, a.ii, a.iii) SEM showing the formation of brittle phases in W. (b) SEM showing micro-crack formation and un-molten particles. (c.i) SEM showing pores formation in W. (c.ii) EDX showing pore formation in W. (The figure composition is adopted from Ref.[23]).

matrix bonding. In addition, the Marangoni convection, small melt pool size, and rapid solidification rates can result in a more uniform distribution of reinforcement in the matrix material.[14,15] Furthermore, the use of AM techniques has broadened the application of refractories which were previously limited by conventional manufacturing. In addition, layer-by-layer printing enables the deposition of coatings/claddings with enhanced microstructures on different substrates to be used in extreme conditions.

Nevertheless, there are certain challenges in the AM of refractory materials, including cracking due to rapid cooling rates, retention of unmolten powders, pore formation and sensitivity to impurities like oxygen that can have an adverse effect on the printability and mechanical properties of refractory materials.[16,17] The oxygen impurities lead to the formation of brittle phases that further deteriorate the processability of these material systems. These brittle phases cannot tolerate residual stresses inherent to the process and the resulting crack formation is detrimental to mechanical properties.[18–22] Some of these challenges are highlighted in Figure 1. Figure 1(a) shows the formation of brittle phases while printing tungsten. Figure 1(b) shows an unmolten W particle and cracking in a single layer print of W and Figure 1(ci,ii) shows the formation of pores in W sample due to the rapid solidification and high viscosity of the molten tungsten.

In addition to the inherent material challenges, specific challenges exist for different AM techniques used to process refractory metals and their carbides. For example, cracking issues tend to be more prevalent in laser-based AM compared to electron beam melting (EBM) because of more oxygen content in the former.[24] In addition, EBM typically exhibits lower level of residual stress than laser-based AM because of pre-heating the materials during the printing processing.

This review article discusses novel approaches like substrate heating, alloying, use of ultrasonic vibration, and laser shaping to improve the AM of refractory metals and their carbides processed using both fusion-based methods (e.g. powder bed fusion, direct energy deposition) and solid-state methods (e.g. binder jetting followed by sintering and cold spray).

Approaches to improve printability of refractories

Substrate heating

In fusion-based AM, the high-temperature processing and rapid cooling rates result in thermal gradients that give rise to residual stresses. These residual stresses often negatively impact the overall performance as they lead to distortion and cracking (at both micro and macro level).[25–27] Cracks may also form because of precipitation hardening, liquation cracking, solidification cracking, or the formation of undesired phases (e.g. brittle intermetallics).[28–30] The microcracking issue becomes more acute for brittle refractories with inherently high ductile to brittle transition temperature (DBTT). For refractory metals like tungsten, the high DBTT around 673 K is a consequence of the limited mobility in screw dislocations within the BCC lattice.[31] Heating the substrate above DBTT and/or temperature below which unwanted brittle phases are formed has been shown to improve printability.[31–34] Especially in the case of EBM, which inherently involves substrate pre-heating during the process, the processability of refractory materials can be enhanced.[35,36]

Figure 2(a) Shows a schematic representation of an experimental setup with substrate heating during the AM process. Figure 2(b) shows the comparison of simulated

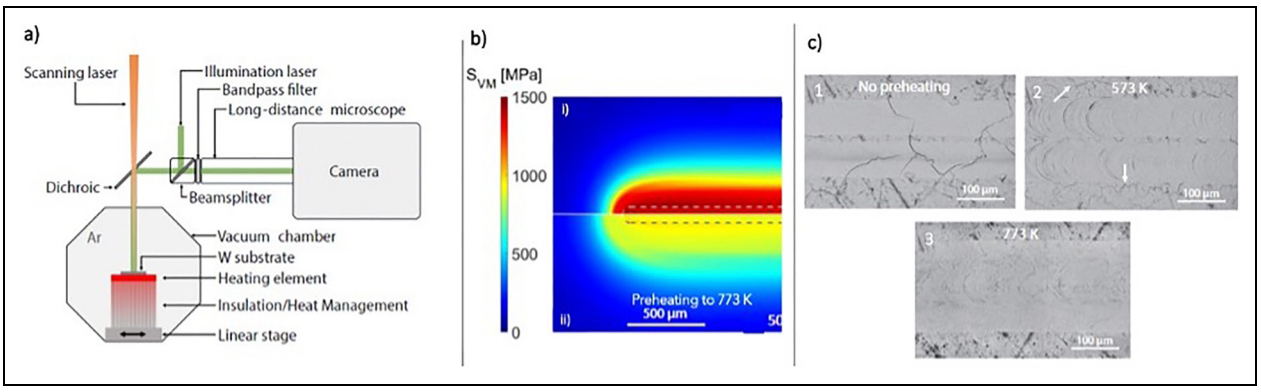

Figure 2. The use of substrate pre-heating to reduce residual stress and microcracking issues. (a) Schematic representation of experimental setup for substrate heating. For single-track remelted W sample. (b) Top surface view of Von Mises residual stress simulations. Without pre-heating (i) and $T_{preheat} = 773$ K (ii), (c, 1–3) top surface of two adjacent scan tracks showing (1) cracking across and adjacent to the scan track without pre-heating, (2) cracking only in the adjacent material for 573 K pre-heating (below DBTT) indicated by white arrows, (3) scan tracks without cracks with 773 K (above DBTT) pre-heating. (The figure composition is adopted from Ref.[31]).

residual stresses without pre-heating (i) and with pre-heating to 773 K (above DBTT of W) (ii) in a single-track remelted W sample. Comparison along the horizontal line of symmetry (the dashed box) shows that pre-heating to 773 K reduces the absolute stresses by 35–40%. Figure 2(c) shows the reduction in cracking with an increase in pre-heating temperature. In case of EBM of W, the high thermal conductivity of W has shown to maintain high substrate temperature (800–950 °C) with low pre-heating temperature of 200 °C. Thus, high heat input in not always needed to maintain a high substrate pre-heating temperature.[37]

The effectiveness of crack reduction depends on the pre-heating temperature as well as the formation of brittle phases, factors influenced by the processing conditions and the quality of feedstock. A study showed that heating the substrate to 673 K did not completely mitigate the cracking issue for both Pure W and W–Ta alloy during the selective laser melting (SLM) process.[38] Similarly, in the case of composites comprising W with a transition metal binder (Ni, Co, Fe, Cu), pre-heating to 673 K during SLM process did not solve the cracking issue. This was attributed to the removal of the binder γ-phase (W–Ni–Fe) at higher processing temperatures and the subsequent formation of a continuous W phase, which is intrinsically brittle.[39] Müller et al.[40] investigated substrate heating to 1273 K during SLM, which reduced both the crack formation and crack density. Although there was a significant reduction in crack density, it was not completely suppressed even at such high pre-heating temperatures due to the difficulty in maintaining low oxygen concentration.[40] Research has indicated that an increase in oxygen concentration to 10, 30 and 50 ppm increases the DBTT of W to 622, 722 and 822 K, respectively.[41] Therefore, in addition to pre-heating temperature, controlling the oxygen content of the feedstock and process environment also plays an important role in crack mitigation. Targeted alloying additions have also been studied to help scavenge oxygen and increase toughness and strength, thereby reducing cracking, which is discussed in the next section.

Alloying to improve the printability

The presence of excess oxygen can be detrimental to the printability of refractory metals thus, different strategies are used to control the oxygen concentration.[42–52] In powder-based AM processes, the presence of oxygen on the powders' surface and in the built atmosphere can lead to the formation of refractory metal oxides that are trapped upon solidification. These oxides typically precipitate at the grain boundaries (GBs) and can promote the formation of intergranular microcracks (Table 1 (1. a)). The lower melting point of oxide phases compared to the matrix phase and their weakening effect on GBs further exacerbate the cracking issues.[53] Alloy addition has been studied to address these challenges. For example, Zr addition in W has been shown to capture oxygen impurities leading to the formation of zirconium oxide nanoparticles and thus improving the room temperature toughness and fracture strength.[54] ZrC addition to W has also been shown to decrease oxygen impurities by the preferential formation of zirconium oxide, which strengthens the GBs by reducing the oxygen concentration at the GBs.[55] Similarly, yttrium addition has been shown to capture excess oxygen through the formation of yttrium oxide during high-temperature processing. Furthermore, the formation of yttrium oxide has been shown to form a large number of low-angle GBs which reduces the propensity for crack propagation in printed parts.[56] Failure to remove oxygen impurity from W leads to formation of tungsten oxide. Tungsten oxide gasification forms nanopores that would accumulate at the GBs. However, adding Nb to W has been shown to form niobium oxide nano-dispersed phases, which can interrupt tungsten oxide formation (Table 1(1, b–d)). Notably, no obvious segregation of nanopores at the GBs was observed, resulting in considerable micro-crack suppression.[57]

The presence of impurities, like nitrogen, carbon, and oxygen, has also been shown to increase the DBTT due to their segregation at GBs. Literature shows that solid

Table 1. Mechanism of improvement of printability of refractory metals and carbides by alloy-addition by microstructural analysis.

Mechanism	Material system	Microstructural analysis
1. Removal of excess oxygen	• Zirconium addition in tungsten[54] • Zirconium carbide addition[55] • Yttrium addition[56] • Niobium addition in tungsten[57]	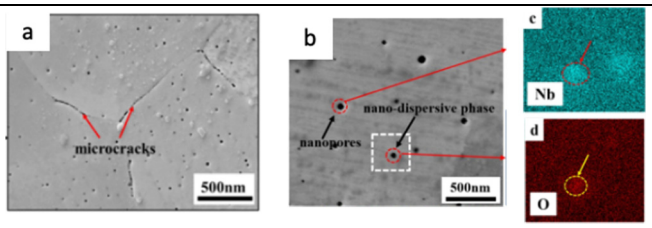 (a) SEM image of microcracks formed by nanopore segregation and aggregation (b) SEM image, (c), (d)EDX map of Nanopore morphology in W–5Nb (adopted from Ref.[57])
2. Reduction in DBTT	• Yttria addition in tungsten[58,61,62] • Rhenium addition in tungsten[59,60]	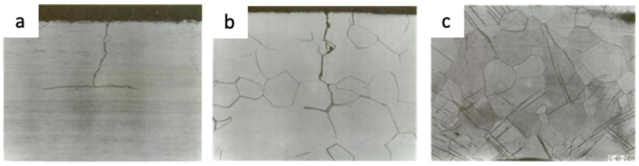 SEM image of annealed and bent to fracture W at 150× magnification (a) 2.5% Re, (b) 2.8% Re, (c) 24% Re Alloy (adopted from Ref.[60])
3. Grain Refinement	• Tantalum addition in tungsten[38] • Zirconium carbide nanoparticles in tungsten[55] • Rhenium addition in tungsten and molybdenum[60] • Titanium addition in tungsten[58,61]	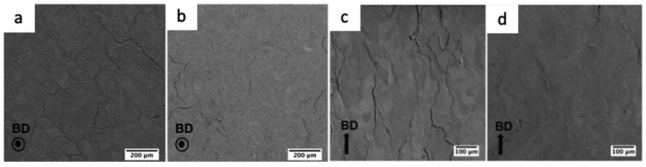 SEM image of (a, b) top surface, (c, d) side view of pure W and W–ZrC (adopted from Ref.[55])
4. Formation of special microstructures	• Niobium addition in tungsten[63] • Tantalum addition in tungsten[64] • Carbon addition in molybdenum[65]	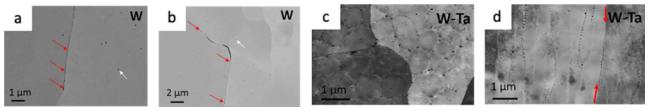 Electron channeling contrast imaging: (a) nanopores segregate at GB in Pure W: (b) nanopores grow into tiny crack in pure W. Nanopores were trapped by cellular structure in W–6Ta, top view (c), side view (d) (adopted from Ref.[64])

solution alloying with elements that have (i) a different crystal structure (FCC or HCP) than the base alloy and (ii) do not have a high DBTT can be used as a strategy to reduce the DBTT of W.[58] Rhenium (HCP crystal structure) is one example that has been shown to reduce the DBTT in W.[59] Table 1 (2. a–c) shows an enhanced reduction in cracking with increasing the percentage of Re in W. Addition of 1.9 wt-% Re in W reduced the DBTT to 491 K whereas the addition of 9.1 wt-% Re reduced the DBTT to 200 K.[60] Similarly, the HCP crystal structure in yttrium also reduces the DBTT, thus making W more processable.[58,61,62]

Grain refinement is another mechanism that has been widely studied to improve the printability of refractory metals and carbides (Table 1(3.)). For example, the addition of tantalum to tungsten has been shown to reduce grain size significantly and reduction in microcracking. The reduction in the grain size, in this case, was due to the constitutional undercooling and segregation of alloying elements.[38] Similarly, the addition of ZrC nanoparticles has also been shown to reduce the cracking issues in W because of grain refinement. (Table 1(3)) shows the top view (a and b) and side view (c and d) of printed W with and without the addition of ZrC. Furthermore, ZrC has also been shown to form a coherent interface with the W matrix, which in turn improves the cohesion between the grain and phase boundaries.[55] In an alternative mechanism, the addition of Re to W has been shown to refine grain size by increasing the recrystallisation temperature, which reduces grain growth during the printing process.[60] In another manner, the addition of liquid titanium has been shown to inhibit grain growth by forming a Ti-rich layer of constant thickness around the W grains.[58] However, due to the formation of inclusions that tend to segregate at the GBs below 600 °C and the rapid oxidation problem above 600 °C, the addition of liquid titanium to W may not be a practical design strategy.[58,61]

Alloying has been shown to form microstructures that improve the mechanical properties of refractory metals. For example, a study on the addition of Nb in W showed that increasing the weight percent of Nb in W transforms

the microstructure from primarily dendritic to a honeycomb structure which enhances the grain and GB strength and reduces crack initiation sites.[63] The use of Ta has also been shown to improve the ductility of W by modifying the microstructure. Nanopores are shown to be segregated to the GBs in pure W (Table 1 (4. a)), which results in the formation of micro cracks (Table 1 (4. B) in the pure W microstructure. On the other hand, the alloy with a 6 wt-% addition of Ta formed a fine, submicron intragranular cellular structure. This microstructure is composed of many interlocked dislocations which help suppress cracking by trapping the nanopores (crack initiation sites) inside the grains, as shown in Table 1 (4. c, d). The cells also served as dislocation sources, and under external load, the dislocation slip facilitated plastic deformation. The residual strain energy was more efficiently absorbed by the plastic deformation, thus reducing crack formation.[64] A similar cellular structure was formed with the addition of 0.45 wt-% C during the laser powder bed fusion (LPBF) process of Mo. Due to constitutional super-cooling, the solidification mode changed from planer to cellular. The cells formed in this case were organised with a misorientation angle between 0 and 0.5 and the adjacent cell colonies were separated by high-angle GBs. This resulted in the change in the fracture mode from inter- to trans-granular thus improving the printability of Mo.[65]

Non-melt-based additive manufacturing

In the previous sections, the use of melt-based AM techniques has been discussed, whereas this section includes some of the non-melt-based metal AM techniques for the production of refractory metals and carbides. Non-melt processes are advantageous as they eliminate the need for melting, resulting in reduced energy consumption, shrinkage and warping issues, and can be applied to a wider range of materials.[66–68] Despite these advantages, there are certain challenges in using non-melt-based techniques. There is a need for post-processing and the resultant grain growth during post-processing is not desirable.[69–71] However, there is ongoing research on creating combined processes to overcome these issues. For example, a study produced WC parts by binder jet[72] AM, then infiltrated the green part with[73] cobalt to minimise shrinkage and grain growth.[73] With an approximate Co content of 25 wt-% shrinkage reduced to within 3% in all directions. Figure 3(a) shows a schematic representation of Binder jet printing followed by melt infiltration. Figure 3(ai) shows Co loaded into WC confinement and heated to processing temperature. Figure 3(aii) shows the infiltration of Co into WC preform using capillary forces. Figure 3(a, iii) and (a, iv) shows the part fully infiltrated with Co to form WC–Co composite structure.[74] Figure 3(b), (c) shows SEM and EDX analysis of the same part. Figure 3(b) shows the WC surrounded by Co (formed in the lower part of the preform) whereas Figure 3(c) shows WC surrounded by a ternary phase consisting of WC–Co and some WC–Co_xW_xC (where x is mostly 3 or 6) formed in the top part of the preform. The formation of ternary phase was depended on the height of the sample, as the diffusion of Co decreases as the distance from Co source increases. Thus, no ternary phase formed at the bottom and a significant amount formed at the top. The formation of ternary phase as shown in Figure 3(c) promotes cracking as it is more brittle than Co phase and thus can be detrimental to the final properties.[75,76] Several other studies also mention the use and advantages of binder jetting followed my melt infiltration for manufacturing net-shaped parts with WC and other refractory carbides.[74–78]

Bound metal deposition (BMD) is another hybrid technique combining powder induction moulding (PIM) and extrusion-based AM to process refractories. This technique

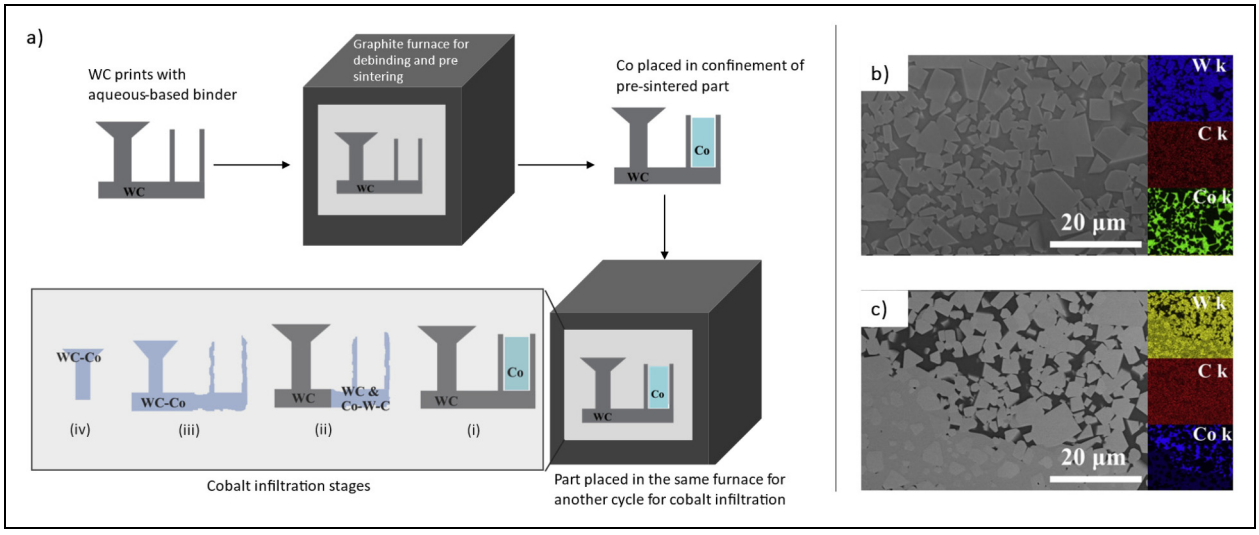

Figure 3. Binder jetting followed by melt infiltration. (a) Schematic showing cermet process flow for binder jet additive manufacturing followed by melt infiltration showing progression of Co infiltration into WC to form WC–Co. For binder jet of WC followed by Co infiltration SEM and EDX analysis showing (b) SEM and EDX analysis of WC–Co microstructure in the lower part of the preform (c) ternary phase formation consisting of WC–Co and WC–Co_xW_xC (where x is mostly 3 or 6) formed in the top part of the preform.[74,76] (The figure composition is adopted from Ref.[76]).

uses a powder mixture with an organic binder which is then converted into precision rods (6 mm diameter and 150 mm length). These rods are fed into an extrusion-based printer to form green parts. Subsequently, a solvent debinding step is conducted to remove a controlled amount of the binder phase, followed by a final sintering cycle.[79] This technique has proven capable of producing parts with high densities (>99.5% dense) and mechanical properties on par with those of commercially available industrial-grade products.[80–83]

Selective laser curing (SLC) is another novel technique that is used for the fabrication of high-temperature carbide composites. This technique involves simultaneous irradiation of powders that induces a curing reaction in the pre-ceramic polymer binder phase. In the absence of binder or the use of polymeric binders, shrinkage is often an effect of subsequent heating treatments such as pyrolysis, which forms the porous part. In SLC, the removal of the pre-ceramic binder phase is not required as the irradiation of the powders and the curing reaction are concurrent. Therefore, the processes occurring simultaneously mitigate the shrinkage induced by pyrolysis. The porous structure is then infiltrated using liquid metal to form a fully dense part.[84] Selective laser sintering (SLS) is used in a similar way to process refractory carbides followed by metal infiltration.[85,86] In SLC, lower temperatures than SLS is required for effective sintering. The absence of a binder phase in SLS requires higher temperatures during processing to trigger the sintering of the ceramic particles. Distinctly, the lower temperature required in SLC results in less thermal gradient-induced damage and produces parts with better dimensional accuracy.[87]

Cold gas-dynamic spray, also known as cold spray, is another non-melt metal AM technique used to process refractory metals by accelerating powdered material towards the substrate by employing a supersonic jet of compressed gas.[88,89] Figure 4(a) shows schematic representation of the cold spray technique.[90] This technique has been shown to form highly dense and hard deposits due to plastic deformation induced strengthening.[91] Studies to understand the bonding mechanism, deposition characteristics, effect of process parameters and heat treatment have been conducted to further advance the field.[92–98] The deposits in cold spray are formed by building blocks known as splats as shown in Figure 4(b) and (c). Due to significant plastic deformation induced during the process, the crystalline structure undergoes lattice rotations[99] and there is an increase in dislocation density. These phenomena form highly refined and elongated grain structure at the inter-splat jetting regions as shown in Figure 4(d) and equiaxed ultrafine nano-grains nested within them as shown in Figure 4(e).[91]

Tantalum produced by the cold spray method shows high strength, attributed to the formation of ultrafine grains and elongated coarse grains. Specifically, the ultimate tensile strength (UTS) of cold-sprayed Ta reaches approximately 485 MPa, surpassing values reported for EBM tantalum at 205 MPa and powder metallurgy-produced tantalum at approximately 310 MPa.[100] While the UTS of cold-sprayed parts falls below that of SLM, which has been reported at around 600–750 MPa, SLM parts exhibit reduced ductility.[101] The crack branching and formation of secondary cracks observed in the cold spray samples indicates an enhanced energy release without substantial propagation of the primary crack. The tantalum printed parts had an average hardness value of 265.97 ± 2.34 HV surpassing the hardness of EBM Ta (110 HV) and powder metallurgy compacted Ta (120 HV).[102]

Additionally, parts processed by the cold spray techniques have been investigated for corrosion resistance.[93–95] This property is especially crucial for refractory metals used in high-performance applications such as aerospace, nuclear energy and defence, as corrosion can compromise the integrity of the part and potentially lead to catastrophic failures.[103–105] Refractory metals like titanium formed by cold spray technique showed good corrosion resistance

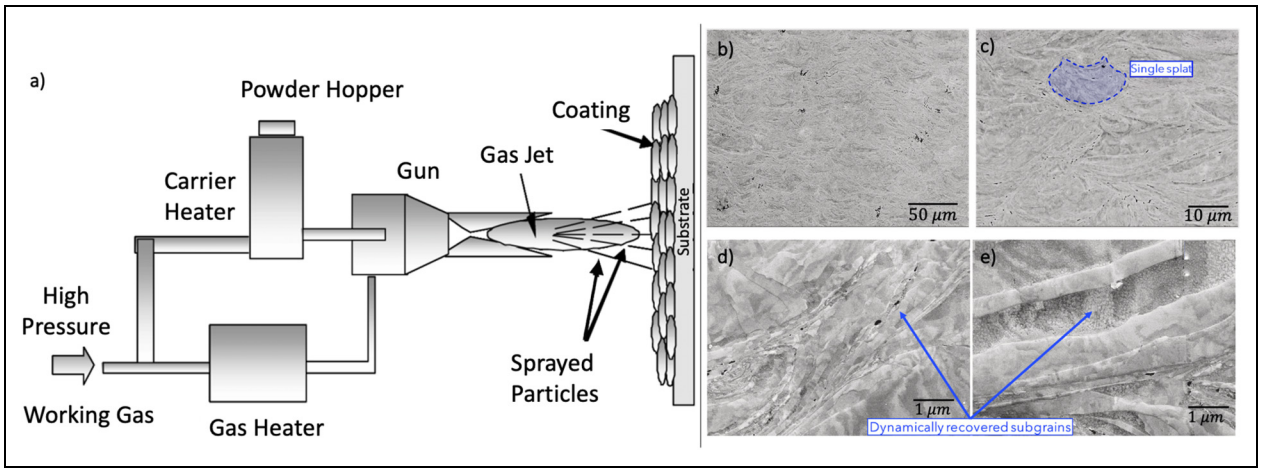

Figure 4. Cold spray of refractory metals and carbides. (a) Schematic of cold spray process. (b–e) Multiscale hierarchical microstructure of cold-sprayed deposit. (b) Monolithic deposit with high integrity and negligible porosity. (c) Splats, the building blocks of the deposit. (d, e) Extensive plastic deformation at the inter-splat jetting regions showing dynamic recovery, with (d) elongated subgrains and (e) nested equiaxed nano-grains. (The figure composition is adopted from Refs.[90,91]).

due to the percolation of corrosion medium through inter-spat boundaries that form a protective oxide layer to prevent bulk titanium from further corrosion. Research has also shown improved corrosion resistance of cold-sprayed samples of tantalum and niobium especially in as-printed conditions . The weight loss percentage of a Ta sample processed with cold spray technique was measured by immersing it in a corrosion medium prepared by adding 12 drops of HF to 50 ml distilled water. Over the period of 5 weeks, the average corrosion rate was as low as 7.5% at a heat treatment temperature of 1500 °C. The average corrosion rate for a Nb sample was 10% under a heat treatment temperature of 500 °C.[104] The presence of defects in cold-sprayed coatings significantly influences their corrosion performance, making the optimisation of processing parameters essential for achieving top-quality coatings with enhanced corrosion resistance. Specifically, employing elevated pre-heating temperatures in cold spray processes can enhance plastic deformation during impact, resulting in denser refractory coatings.[105]

Hardness is another key property for refractory coatings like those made of WC–Co. The hardness of WC–Co samples produced by SLM and EBM is around 1500 HV.[9] For samples produced by binder jetting the hardness value is lower and reported to be around 1300–1400 HV.[106] For cold spray coatings, the hardness value can be as high as 1600–2000 HV which gives this technique an edge over other AM techniques to deposit refractory coatings with high hardness values.[107]

The cold spray technique has a lot of potential for use in oxygen sensitive materials. When powder feedstock strikes the substrate with a very high velocity, there are high chances of breaking the oxide layer on the powder, thus reducing the oxygen content in the final coating. This is advantageous for refractory material systems since the presence of oxygen forms brittle oxide phases that lead to cracking issues. Additionally, high melting temperature refractory metals can be processed by cold spray technique, offering a more energy and material-efficient processing route as it does not require heating the material to the extremely high inherent melting temperatures.[108,109] Nevertheless, there are certain challenges in using the cold spray technique for processing refractory metals and carbides including the brittle nature of these materials causing reduced coating quality due to limited plastic deformation. While increasing the temperature can assist in deposition, it can also lead to oxidation of the particles if not processed in a controlled environment. There is a lot of room for innovation in cold- spray and other non-melt-AM processes to address the challenges in the processing of refractory metals and their carbides to achieve the desirable properties.

Future trends

AM is a fast-evolving field where continuous advancements are being made to solve the materials and manufacturing challenges we are currently facing. In the previous sections, we addressed some of the challenges in the AM of refractory alloys and their carbides, including microcracking, brittle oxide phase formation, and their characteristic DBTT. In this section, we will discuss some novel trends in AM to mitigate these challenges, which have the potential to be adopted for processing refractory metals and carbides.

In-situ reactive printing

In-situ reactive printing relies on in-situ chemical reactions of elemental powder blends instead of using pre-alloyed powders to produce new material systems.[110] There are several advantages of in-situ reaction-based AM, including thermodynamically stable reinforcements, strong matrix to reinforcement bonding, and improved properties due to homogeneous dispersion of the reinforcements.[111] Several studies have been conducted to explore and utilise the advantages of in-situ alloying strategy in the AM of MMCs.[112–114]

Zang et al.[115] demonstrated a novel way of in-situ processing refractory metals and their carbides which has great potential to be extended to AM process. As shown in Figure 5, steam cracker tar was used as a binder and light absorber as it has a significantly lower attenuation coefficient than metals. As a result, it was possible to use a lower laser power (<2 W CO_2 laser in air) to process refractory metals. In addition, it was possible to execute the process in air without the need for a vacuum or an inert atmosphere, as tar has a high affinity to oxygen which can suppress the formation of metal oxides. This technique has the potential to overcome undesirable oxide formation in refractory metals and MMCs.[115] Furthermore, sourcing refractory carbide feedstock is challenging, but utilising in-situ reactions to generate carbides may offer the opportunity to investigate novel refractory carbide material systems.

In another study, a thermally driven reaction of a metal/metal oxide mixture with CH_4 gas was carried out, resulting in the in-situ production of metal carbide. The reaction mixture was ball-milled to increase the adsorption of CH_4 gas and H_2 gas was added to obtain better carbide yield. Figure 6(a) shows schematic of high-volume, low-pressure (HVLP) air-assisted slurry spray deposition for low pressure deposition of the feedstock film on a substrate. Figure 6(b) shows the schematic of the setup for carrying out the gas–solid reaction. The conversion of a metal to a ceramic (Cr to Cr_2C_3) resulted in volume expansion, while the conversion of metal oxide to non-oxide ceramics (Cr_2O_3 to Cr_3C_2) resulted in volume reduction. In all, the reaction led to an isovolumetric Cr_3C_2 formation. The isovolumetric conversion can suppress cracking and thus makes this approach appealing for fabricating non-oxide ceramics and potentially refractory carbides.[116] Figure 6(c) shows SEM of Cr/Cr_2O_3 precursor film where the large particles show Cr embedded in a population of smaller Cr_2O_3. SEM analysis of the final Cr_2C_3 formed is presented in Figure 6(d) and (e). The low magnification image in Figure 6(d) reveals a moderately homogeneous microstructure that formed during the process. Meanwhile, the higher magnification image in Figure 6(e) shows the formation of a continuous network of Cr_2C_3, with the Cr particles increasing in volume

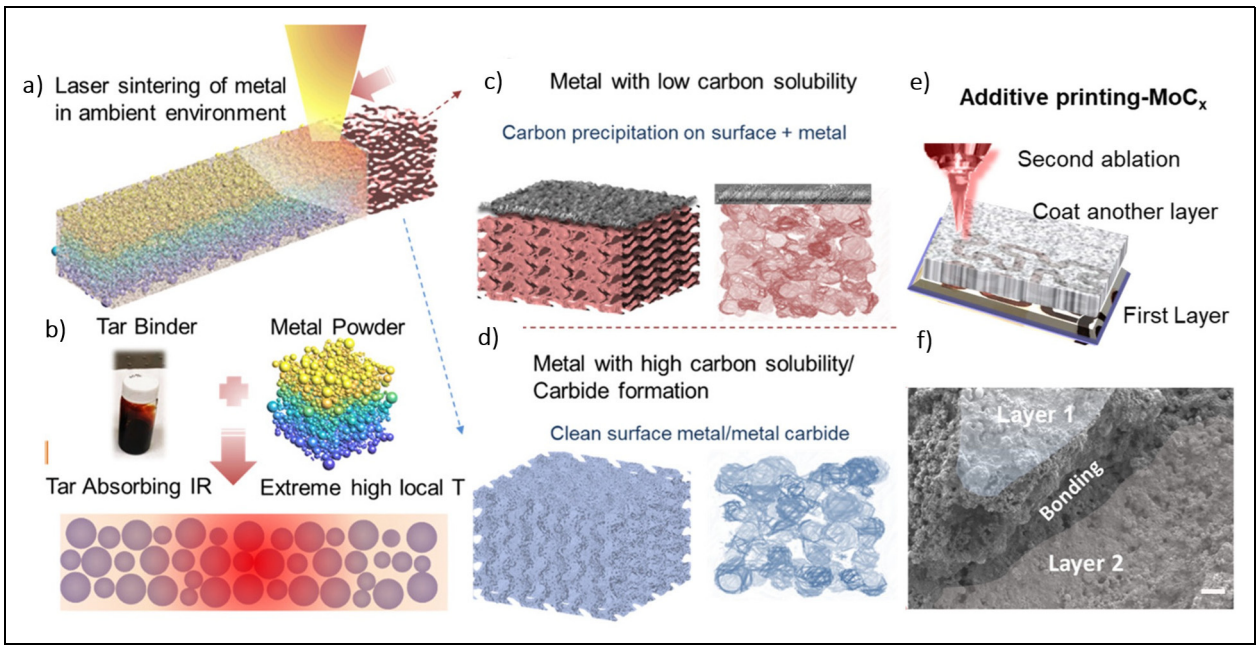

Figure 5. Schematic of laser annealing of refractory metal carbides using petroleum tar as light-absorbing binder, (a, b) illustration of laser-sintered metal thin film with tar-binder. (c) Carbon segregation on metals with low carbon solubility like Al and Cu after laser sintering. (d) Metals with high carbon solubility led to a smooth surface after sintering; refractory metals Mo and W form carbides. (e) Schematic of double layer metal printing using tar. (f) SEM of printed double layer molybdenum carbide highlighting bonding interface. (The figure composition is adopted from Ref.[115]).

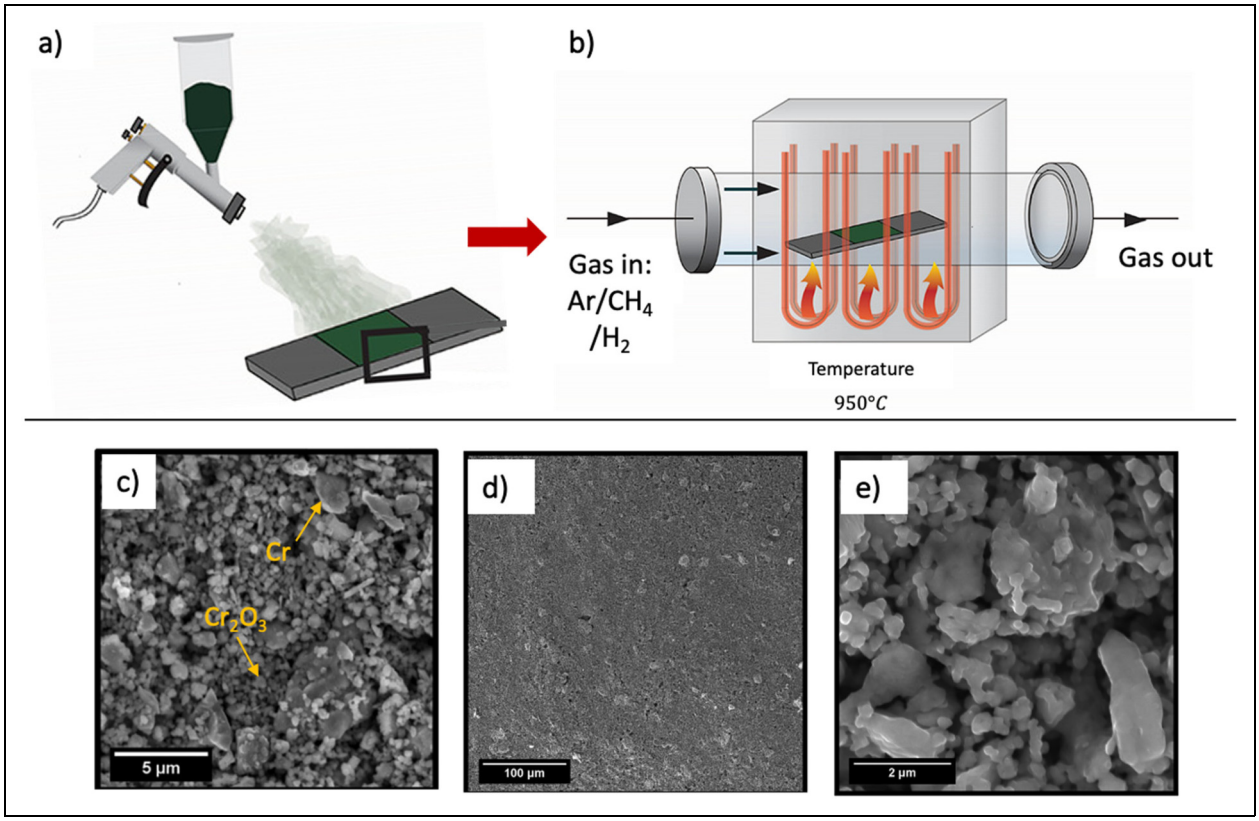

Figure 6. Isovolumetric synthesis Cr_2C_3. (a) HLVP spray deposition for feedstock film deposition. (b) Gas–solid reaction of Cr/Cr_2O_3 precursor film with CH_4 and H_2. (c) SEM of Cr/Cr_2O_3 precursor film where large particles are Cr embedded in smaller Cr_2O_3 particles. SEM showing final formed Cr_3C_2. (d) Low magnification showing moderately homogeneous microstructure. (e) High magnification showing particle connectivity forming a continuous network. (The figure composition is adopted from Ref.[116]).

as they are converted into Cr_3C_2. The smaller Cr_2O_3 particles, on the other hand, coalesce as they are converted into Cr_3C_2.[116] There is scope of research in further using this technique for processing refractory material systems.

A challenge associated with this method is the difference between the laser absorptivity for metals and their oxides and thus, processing parameters needs to be optimised accordingly. Also, effective laser penetration depth depends on size and thermal conductivities of feedstock. Choosing the appropriate particle size is crucial for effectively implementing this technique to enhance conversion rates and minimise coalescence.[117] This technique offers a significant benefit, particularly in the processing of refractory metals and carbides, as the precursors can undergo conversion below their melting points, allowing for processing at lower laser energies. However, while efforts are underway to extend this technique to other refractory metal carbide material systems such as HfC and TaC, the selection of appropriate precursors and the understanding and controlling of the processing parameters remain a challenge.[118]

Unconventional scanning strategies

Laser beam shaping. A recent trend in metal AM is the use of laser beam shaping to engineer light-matter interactions that could tailor the microstructure and properties of printed parts.[119–123] Adaptive beam shaping enables tailoring the beam power distribution that could enable a modification of heat input and also influence the melting and solidification behaviour.[124] Figure 7(a) shows a schematic representation of the laser beam shaping process where polarisation and altering the amplitude and phase are being used to modify a conventional beam.[125] Laser beam shaping has been shown to promote microstructural changes using predictive simulations that combine ultra-fast hydrodynamic melt flow, full laser tracing, and a cellular automated method for grain growth.[126] Figure 7(b) compares the laser-metal interactions under the effect of Gaussian beam and elliptical beam modeled using ALE3D finite element code. Here the Gaussian beam forms a deeper depression relative to the elliptical beam, which can have more of an effect on the local thermal gradient and microstructure. Shi et al.[126] found a strong correlation between melt pool geometry, nucleation propensity and beam-shaped geometry when assessing the circular Gaussian beam, transverse elliptical beam and longitudinal elliptical beam.[126] Simulations show that at a similar laser power and scanning speed, the temperature gradient is usually most steep in the scanning direction using the transverse elliptical profile (68×10^3 K/cm), followed by the Gaussian (50×10^3 K/cm) and longitudinal elliptical (47×10^3 K/cm) profiles. This is due to the fact that the centreline of tracks melted by the longitudinal elliptical profile experience heating longer than those melted by the transverse elliptical profile. Figure 7(c) shows an example of SS316 microstructure highlighting the reduction in the major axis length of the grains when processed using an elliptical beam.

Bessel-shaped beam profiles have also been shown to stabilise melt pool turbulence and increase the time for solidification by reducing thermal gradients.[119] Figure 8 shows the effect of Bessel beam and Gaussian beam on melt pool size where Figure 8(bi,ii) shows melt pool size plotted as a function of velocity, beam diameter and volumetric energy density. The melt pool generated by Bessel

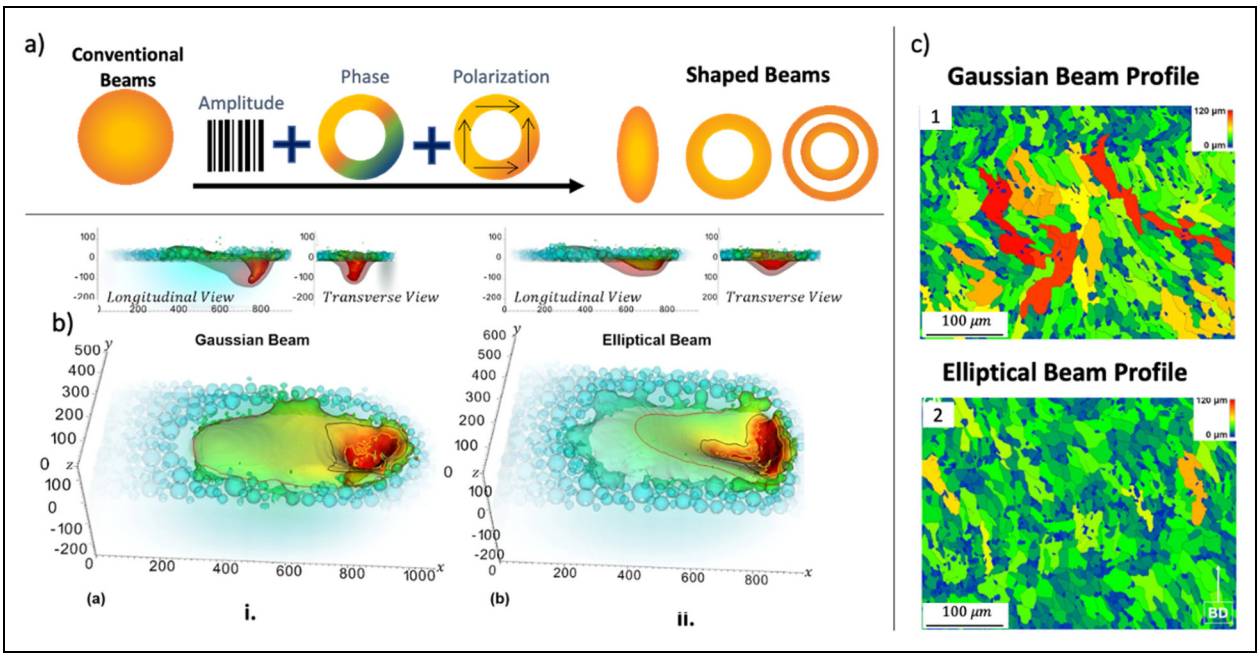

Figure 7. Schematic representing laser-shaping strategy to aid additive manufacturing. (a) Schematic demonstrating the laser beam shaping by tailoring the amplitude, phase and polarisation of light. (b) ALE3D simulation of single tracks for (i) Gaussian beam shape and (ii) elliptical beam shape (pseudo-colour range corresponds to temperature variation). (c) Microstructures of cubes built with (1) Gaussian beam and (2) elliptical beam. Grains are coloured by major axis length in (1, 2). (The figure composition is adopted from Refs.[119,125]).

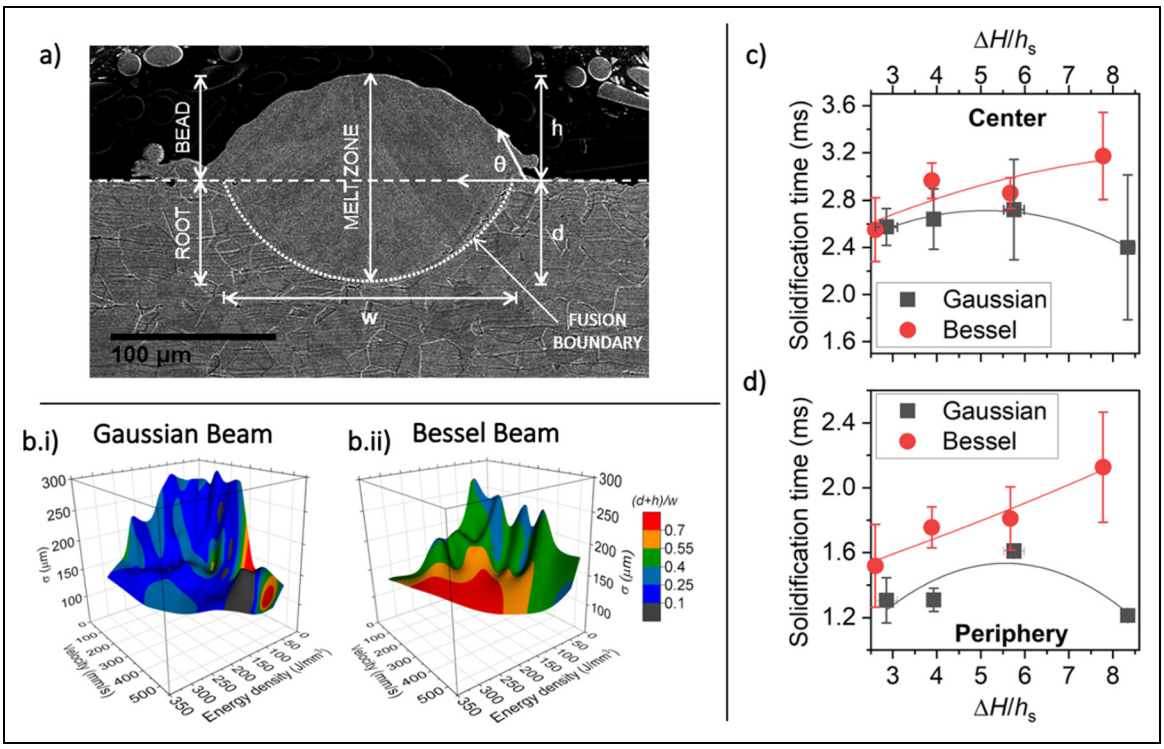

Figure 8. Effect of laser beam shaping on the melt pool characteristics. (a) Typical transverse melt track cross-section dimensions labeled. Here, h = bead height, d = substrate penetration depth, w = maximum width of track root, θ = contact angle. b.i,ii) shows effect of beam shaping on melt pool dimensions. Melt pool size is plotted as a function of velocity, beam diameter and volumetric energy density for (b.i) Gaussian Beam and (b.ii) Bessel beam. Solidification time for Gaussian and Bessel beams at (c) centre and (d) edge of the fluctuating melt pool. (The figure composition is adopted from Ref.[127]).

beam is larger (deeper and narrower) and has a monotonic variation for a broader parameter space as compared to that produced by Gaussian beam. Figure 8(c) and (d) shows the solidification time is more for Bessel beams as compared to Gaussian beams at both the centre and periphery of the melt pool. The melt pool solidification time is plotted as a function of energy density ($\Delta H/hs$) which is the ratio of absorbed energy density to the volumetric melting enthalpy. Bessel beams stabilise the melt pool turbulence and increase the time for melt pool solidification, leading to reduced thermal gradients. While these studies are mainly focused on non-refractories, the reduction in thermal gradient achieved through beam shaping can be leveraged in the printing of refractory metals and carbides.[127]

Despite its benefits, the laser beam shaping has several limitations, such as the need to choose an appropriate oscillation frequency since some material systems are better at absorbing low frequencies while others are better at absorbing high frequencies. In addition, slow processing speeds are a result of frequency limitations and there is limited flexibility to generate different shapes due to current constraints in optical equipment and technology.[128–131] The evaluation of different beam profiles for enhancing metal AM is ongoing and could potentially enhance the processing of refractory materials.

Multi-laser systems. Multi-laser AM is an advanced technology that simultaneously employs multiple laser beams in 3D printing processes. This innovation offers several advantages, including increased throughput and the ability to manipulate thermal history, thereby influencing microstructures and residual stress development in printed parts.[132] Prior studies have shown that while the peak temperature of the melt pool is relatively insensitive to changes, the magnitudes of temperature gradients are highly sensitive to factors such as scan strategy and the number of lasers used. Achieving an optimal scan strategy depends on various factors, including the dimensions of layers, laser wavelength, synchronicity, power and speed. Additional work, both computational and experimental, is required to optimise these process parameters to attain specific thermal profiles.[133] This technique has the potential to tightly control heat input and distribution, thus reducing thermal stresses and enhancing the processability of refractory metals and carbides.[134]

Ultrasonic vibration

Ultrasonic vibration in AM has been used to improve the printability of refractory materials and other material systems.[135–148] Figure 9(a) shows a schematic of an ultrasonic vibration setup integrated with laser-based AM process. The introduction of high-intensity ultrasonic vibrations for microstructure modification has been studied in the literature to understand the advantages of ultrasonic cavitation, dendrite fragmentation, and acoustic streaming.[149–156] Zhao et al.[157] used ultrasonic vibration-assisted laser cladding to process WTaNbMo refractory alloy. Ultrasonic

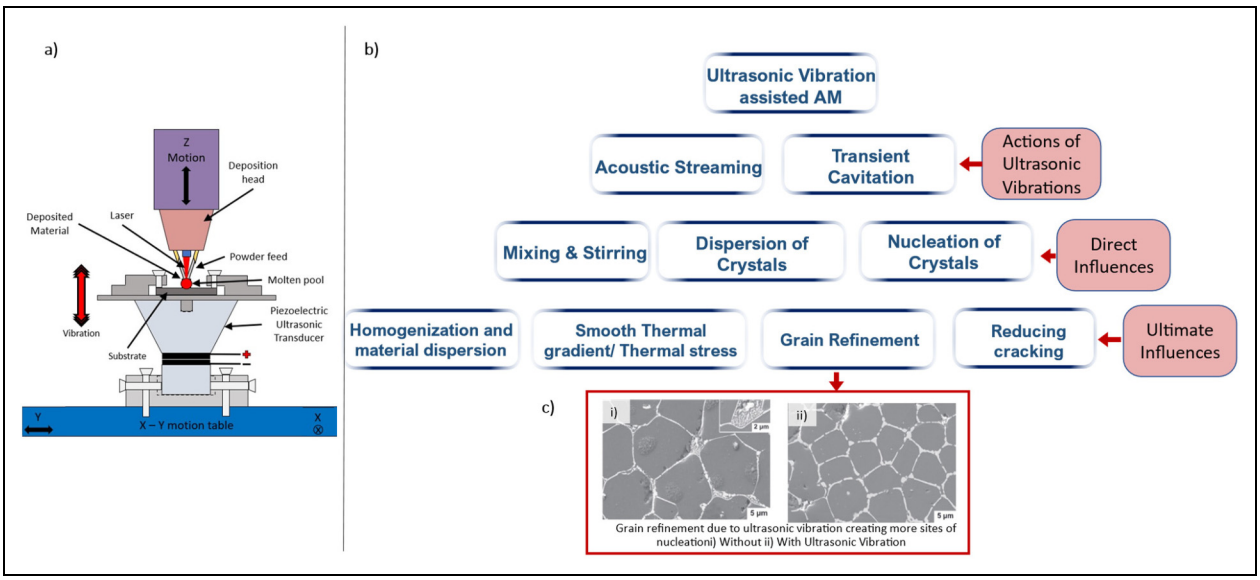

Figure 9. Ultrasonic vibration strategy for additive manufacturing of refractory metals and carbides. (a) Schematic representation of experimental setup for ultrasonic vibration-assisted additive manufacturing. (b) Flow chart showing actions and influences of ultrasonic vibration-assisted melting and solidification processes. (c) Grain refinement. (The figure composition is adopted from Ref.[136]).

vibration improved the homogeneity of the microstructure, decreased grain size from 0.48 to 0.30 μm^2, and improved microhardness from 753 to 980 Hv and reduced the wear rate by 15% at room temperature.[157] The improvement in printability by this technique can be attributed to the acoustic flow effect, which is the combination of circulation, laminar and turbulent flow, and stirring. Thus, the acoustic flow effect reduces macro-segregation and enhances dispersion by the cavitation effect.[158] Figure 9(b) shows a flow chart that illustrates the actions and ultimate influences of ultrasonic vibration. Acoustic streaming and transient cavitation are the direct actions of ultrasonic vibrations. Acoustic streaming is a steady flow generated in the liquid due to the absorption of acoustic oscillation. As a result, mixing, stirring and dispersion of crystals will occur, which can reduce the thermal stresses and homogenise the material. Transient cavitation facilitates the formation, growth, pulsation and collapse of micro-sized bubbles. This mechanism helps in the nucleation and dispersion of crystals, which can induce grain refinement (as shown in the microstructure in Figure 9(c)) and may suppress cracking. Thus, the use of ultrasonic vibrations for the AM of refractory metals and carbides could potentially overcome the challenges like precipitation of brittle oxide phases at the GBs leading to microcracking.

Although the use of ultrasonic vibration to aid metal AM has now been widely studied, work is needed to overcome certain challenges to couple ultrasonic vibrations to the melt pool and to understand the attenuation of ultrasonic vibrations through different substrates. Most of the studies mentioned in the literature coupled the ultrasonic setup to the build plate and thus do not allow the build plate to be clamped which in turn could lead to distortion in larger parts. Also, if the ultrasonic vibration systems are directly attached to the build plate as shown in Figure 9(a), it could lead to excessive heating of the electronics thus could lead to their damage. In AM techniques like LPBF the use of ultrasonic vibrations is challenging as it may disrupt the layer of powder after recoating.[159] Studies have shown that ultrasonic vibrations tend to attenuate more with an increase in distance,[160] an increase in the density of medium,[161] and an increase in the temperature.[162,163] Therefore, when dealing with refractory powders that have high density and require high processing temperatures, it is crucial to conduct an in-depth analysis of the attenuation of ultrasonic vibrations used to aid the AM process.

Summary and perspectives

With the advancement in the space, energy and defence sectors, the need to develop novel materials that can withstand extreme environments has become critically important. Refractory metals and their carbides are promising materials for these applications but have certain challenges that make them difficult to process. These challenges include requirement of high processing temperatures, formation of brittle oxide phases that segregate at GBs leading to cracking, high DBTT, and inherent brittle nature leading to micro-crack formation. Improvements and innovations in AM have the potential to both solve these challenges and develop novel material systems with even better properties. This paper gives a comprehensive overview of the present advancements in AM and the future research trends in this field. Some challenges and future scopes in research in the discussed approaches to aid the AM of refractory metals, and their carbides are:

1. The application of substrate heating has been demonstrated to mitigate cracking during the processing of refractory materials. However, the appropriate preheating temperature is contingent on the materials' DBTT, which is influenced by feedstock impurities. The majority of studies in this field have employed

custom laboratory-scale setups and require additional research to establish scalability. It is also worth noting that the elevated temperatures required to achieve the mentioned benefits are demanding and would result in high energy consumption, thereby increasing the manufacturing cost.

2. We discussed different mechanisms by which alloy addition can improve the printability of refractory metals and their carbides. For instance, some alloying elements can effectively eliminate excess oxygen present in feedstock. However, one of the major challenges with this approach is to ascertain if the resulting oxide phase has any negative impact on the microstructure, such as the formation of a brittle phase or porosity due to oxide phase evaporation. Ultimately, the microstructure's formation is contingent on the material system and processing parameters, making it difficult to generalise. There is ample room to investigate new chemistries for grain refinement, reduction in DBTT and improving the printability of refractory material systems. However, procuring refractory metal powders for custom chemistries is challenging because of the limited number of high-quality suppliers.
3. The use of in-situ reactions is promising for reducing the necessary processing temperatures for refractory material systems and generating new high-temperature phases through controlled reactions. However, such reactions may result in the formation of undesired phases which can deteriorate the properties of the printed part. Furthermore, controlling the reaction becomes difficult due to the fast-cooling rates in most AM processes.
4. Laser beam shaping has significant potential for controlling the melt pool, microstructure, and properties of 3D printed parts, particularly refractory materials. However, there are hardware limitations to overcome, such as slow processing due to frequency limitations and limited flexibility in choosing beam shapes due to current optical equipment constraints. To address these limitations, it is necessary to explore various strategies, and there is a considerable scope for further research in this field. Using good quality beam delivery systems can help minimise the beam distortion, increase the beam shaping accuracy and reduce the energy losses due to beam scattering. Also, the frequency of the laser beam plays a crucial role in optimising the laser beam shaping process. For example, high-frequency laser beams have a better resolution but are very complex and expensive which limits their use. Further computational and experimental research is needed to learn more about the impact of beam shaping and apply it to process refractory material systems.
5. Utilising ultrasonic vibration in AM has the potential to homogenise material dispersion, smooth thermal gradients, refine grains and reduce microcracking. This technique has been widely used in metal AM and now been expanded to refractory material systems. However, most of the ultrasonic systems being used currently are connected directly to the substrate and thus the substrate is not typically clamped. This can result in distortion while printing taller parts. Additionally, techniques like PBF cannot use the ultrasonic vibration assistance since it may disrupt the powder layer. The intensity of ultrasonic vibrations decreases with increased distance away from the source, so this technique becomes less efficient in higher layers. Moreover, high temperatures are often necessary for printing refractory metals and carbides in melt-based AM, making it challenging to design electronics that can withstand such high temperatures during printing. Furthermore, high-temperature processing would attenuate the ultrasonic vibrations, so more studies need to be conducted to optimise the transfer of ultrasonic vibrations to assist the printing process.

The interest in refractory metals and carbides has increased significantly over the past few years because of the demand for ultra-high-temperature materials with better properties. By understanding the current capabilities of AM, highlighting the pertinent challenges of the materials, and addressing future research trends, it is reasonable to expect novel material systems with enhanced properties in the near future.

Declaration of conflicting interests

The authors declared no potential conflicts of interest with respect to the research, authorship and/or publication of this article.

Funding

The authors disclosed receipt of the following financial support for the research, authorship and/or publication of this article: The authors gratefully acknowledge the funding and collaboration provided by the Jet Propulsion Lab, California Institute of Technology, under contract with NASA, for the research on refractory metals and carbide systems. This work was partially supported by the Cornell Center for Materials Research (CCMR) with funding from the NSF MRSEC program (DMR-1719875). AM acknowledges financial support from National Science Foundation CAREER Award (CMMI-2046523) and Office of Naval Research Young Investigator Award (N00014-22-1-2420).

References

1. Ren C, Enneti R and Ouyang G. Refractory materials for corrosive or high-temperature environments. *JOM* 2022; 74: 4305–4306.
2. Humphry-Baker SA, Ramanujam P, Smith GDW, et al. Ablation resistance of tungsten carbide cermets under extreme conditions. *Int J Refract Metals Hard Mater* 2020; 93: 105356.
3. Wuchina E, Opila E, Opeka M, et al. UHTCs: ultra-high temperature ceramic materials for extreme environment applications. *Electrochem Soc Interface* 2007; 16: 30.
4. Mireles O. Additive manufacture of refractory metals for aerospace applications. In *AIAA Propulsion and Energy 2021 Forum*. Reston, VI: American Institute of Aeronautics and Astronautics; 2021, pp.1–9.
5. Satya Prasad VV, Baligidad RG and Gokhale AA. Niobium and other high temperature refractory metals for aerospace

applications. *Aerosp Mater Mater Technol* 2017; 1: 267–288.
6. Garcia-Ayala EM, Tarancon S, Gonzalez Z, et al. Processing of WC/W composites for extreme environments by colloidal dispersion of powders and SPS sintering. *Int J Refract Metals Hard Mater* 2019; 84: 105026.
7. Marinelli G, Martina F, Lewtas H, et al. Functionally graded structures of refractory metals by wire arc additive manufacturing. *Sci Technol Weld Join* 2019; 24: 495–503.
8. Lee WE, Zhang S and Karakus M. Refractories: controlled microstructure composites for extreme environments. *J Mater Sci* 2004; 39: 6675–6685.
9. Konyashin I, Hinners H, Ries B, et al. Additive manufacturing of WC–13%Co by selective electron beam melting: achievements and challenges. *Int J Refract Metals Hard Mater* 2019; 84: 105028.
10. Silvestroni L, Pienti L, Guicciardi S, et al. Strength and toughness: the challenging case of TaC-based composites. *Compos B Eng* 2015; 72: 10–20.
11. Guo W, Liu B, Liu Y, et al. Microstructures and mechanical properties of ductile NbTaTiV refractory high entropy alloy prepared by powder metallurgy. *J Alloys Compd* 2019; 776: 428–436.
12. Morales R, Aune RE, Seetharaman S, et al. The powder metallurgy processing of refractory metals and alloys. *JOM* 2003; 55: 20–23.
13. Liu B, Wang J, Chen J, et al. Ultra-high strength TiC/refractory high-entropy-alloy composite prepared by powder metallurgy. *JOM* 2017; 69: 651–656.
14. Behera MP, Dougherty T and Singamneni S. Conventional and additive manufacturing with metal matrix composites: a perspective. *Procedia Manuf* 2019; 30: 159–166.
15. Dadkhah M, Mosallanejad MH, Iuliano L, et al. A comprehensive overview on the latest progress in the additive manufacturing of metal matrix composites: potential. Challenges, and feasible solutions. *Acta Metallurg Sin (Engl Lett*) 2021; 34: 1173–1200.
16. Gludovatz B, Wurster S, Weingärtner T, et al. Influence of impurities on the fracture behaviour of tungsten. *Philos Mag* 2011; 91: 3006–3020.
17. Guo M, Gu D, Xi L, et al. Selective laser melting additive manufacturing of pure tungsten: role of volumetric energy density on densification, microstructure and mechanical properties. *Int J Refract Metals Hard Mater* 2019; 84: 105025.
18. Reichardt A, Dillon RP, Borgonia JP, et al. Development and characterization of Ti–6Al–4V to 304L stainless steel gradient components fabricated with laser deposition additive manufacturing. *Mater Des* 2016; 104: 404–413.
19. Mukherjee T, Zuback JS, De A, et al. Printability of alloys for additive manufacturing. *Sci Rep* 2016; 6: 19717.
20. Manvatkar V, De A and DebRoy T. Heat transfer and material flow during laser assisted multi-layer additive manufacturing. *J Appl Phys* 2014; 116: 124905.
21. DebRoy T, Wei HL, Zuback JS, et al. Additive manufacturing of metallic components – process, structure and properties. *Prog Mater Sci* 2018; 92: 112–224.
22. Blakey-Milner B, Gradl P, Snedden G, et al. Metal additive manufacturing in aerospace: a review. *Mater Des* 2021; 209: 110008.
23. Xie J, Lu H, Lu J, et al. Additive manufacturing of tungsten using directed energy deposition for potential nuclear fusion application. *Surf Coat Technol* 2021; 409: 126884.
24. Talignani A, Seede R, Whitt A, et al. A review on additive manufacturing of refractory tungsten and tungsten alloys. *Addit Manuf* 2022; 58: 103009.
25. Kruth J-P, Deckers J, Yasa E, et al. Assessing and comparing influencing factors of residual stresses in selective laser melting using a novel analysis method. *Proc Inst Mech Eng B J Eng Manuf* 2012; 226: 980–991.
26. Li C, Liu ZY, Fang XY, et al. Residual stress in metal additive manufacturing. *Procedia CIRP* 2018; 71: 348–353.
27. Wu AS, Brown DW, Kumar M, et al. An experimental investigation into additive manufacturing-induced residual stresses in 316L stainless steel. *Metall Mater Trans A* 2014; 45: 6260–6270.
28. Attallah MM, Jennings R, Wang X, et al. Additive manufacturing of Ni-based superalloys: the outstanding issues. *MRS Bull* 2016; 41: 758–764.
29. Carter LN, Attallah MM and Reed RC. Laser powder bed fabrication of nickel-base superalloys: influence of parameters; characterisation, quantification and mitigation of cracking. In *Superalloys 2012*. Hoboken, NJ: John Wiley & Sons, Inc.; 2012; 577–586.
30. Bi G and Gasser A. Restoration of nickel-base turbine blade knife-edges with controlled laser aided additive manufacturing. *Phys Procedia* 2011; 12: 402–409.
31. Vrancken B, Ganeriwala RK, Martin AA, et al. Microcrack mitigation during laser scanning of tungsten via preheating and alloying strategies. *Addit Manuf* 2021; 46: 102158.
32. Lu X, Cervera M, Chiumenti M, et al. Residual stresses control in additive manufacturing. *J Manuf Mater Process* 2021; 5: 138.
33. Wu Q, Mukherjee T, De A, et al. Residual stresses in wire-arc additive manufacturing – hierarchy of influential variables. *Addit Manuf* 2020; 35: 101355.
34. Sadhu A, Choudhary A, Sarkar S, et al. A study on the influence of substrate pre-heating on mitigation of cracks in direct metal laser deposition of NiCrSiBC–60%WC ceramic coating on Inconel 718. *Surf Coat Technol* 2020; 389: 125646.
35. Ellis EAI, Sprayberry MA, Ledford C, et al. Processing of tungsten through electron beam melting. *J Nucl Mater* 2021; 555: 153041.
36. Leung CLA, Tosi R, Muzangaza E, et al. Effect of preheating on the thermal, microstructuraland mechanical properties of selective electron beam melted Ti–6Al–4V components. *Mater Des* 2019; 174: 107792.
37. Yang G, Yang P, Yang K, et al. Effect of processing parameters on the density, microstructureand strength of pure tungsten fabricated by selective electron beam melting. *Int J Refract Metals Hard Mater* 2019; 84: 105040.
38. Iveković A, Omidvari N, Vrancken B, et al. Selective laser melting of tungsten and tungsten alloys. *Int J Refract Metals Hard Mater* 2018; 72: 27–32.
39. Iveković A, Montero-Sistiaga ML, Vanmeensel K, et al. Effect of processing parameters on microstructure and properties of tungsten heavy alloys fabricated by SLM. *Int J Refract Metals Hard Mater* 2019; 82: 23–30.
40. Müller Av, Schlick G, Neu R, et al. Additive manufacturing of pure tungsten by means of selective laser beam melting with substrate preheating temperatures up to 1000 ∘C. *Nucl Mater Energy* 2019; 19: 184–188.
41. Stephens JR. *Effect of oxygen on mechanical properties of tungsten*. Cleveland, OH, USA: National Aeronautics and Space Administration, 1963.
42. Li N, Huang S, Zhang G, et al. Progress in additive manufacturing on new materials: a review. *J Mater Sci Technol* 2019; 35: 242–269.
43. Kh M, Khodabakhshi F, Kashani-bozorg SF, et al. A review on metallurgical aspects of laser additive manufacturing

(LAM): stainless steels, nickel superalloys, and titanium alloys. *J Mater Res Technol* 2022; 16: 1029–1068.
44. Peters AB, Zhang D, Nagle DC, et al. Reactive two-step additive manufacturing of ultra-high temperature carbide ceramics. *Addit Manuf* 2023; 61: 103318.
45. Hancock D, Homfray D, Porton M, et al. Refractory metals as structural materials for fusion high heat flux components. *J Nucl Mater* 2018; 512: 169–183.
46. Herzog D, Seyda V, Wycisk E, et al. Additive manufacturing of metals. *Acta Mater* 2016; 117: 371–392.
47. Awasthi PD, Agrawal P, Haridas RS, et al. Mechanical properties and microstructural characteristics of additively manufactured C103 niobium alloy. *Mater Sci Eng A* 2022; 831: 142183.
48. Popov Vv, Grilli ML, Koptyug A, et al. Powder bed fusion additive manufacturing using critical raw materials: a review. *Materials* 2021; 14: 909.
49. Bermingham MJ, StJohn DH, Krynen J, et al. Promoting the columnar to equiaxed transition and grain refinement of titanium alloys during additive manufacturing. *Acta Mater* 2019; 168: 261–274.
50. Moghaddam AO, Shaburova NA, Samodurova MN, et al. Additive manufacturing of high entropy alloys: a practical review. *J Mater Sci Technol* 2021; 77: 131–162.
51. Fernandez-Zelaia P, Ledford C, Ellis EAI, et al. Crystallographic texture evolution in electron beam melting additive manufacturing of pure molybdenum. *Mater Des* 2021; 207: 109809.
52. Liu M, Zhang J, Chen C, et al. Additive manufacturing of pure niobium by laser powder bed fusion: microstructure, mechanical behavior and oxygen assisted embrittlement. *Mater Sci Eng A* 2023; 866: 144691.
53. Braun J, Kaserer L, Stajkovic J, et al. Molybdenum and tungsten manufactured by selective laser melting: analysis of defect structure and solidification mechanisms. *Int J Refract Metals Hard Mater* 2019; 84: 104999.
54. Xie ZM, Liu R, Fang QF, et al. Spark plasma sintering and mechanical properties of zirconium micro-alloyed tungsten. *J Nucl Mater* 2014; 444: 175–180.
55. Li K, Wang D, Xing L, et al. Crack suppression in additively manufactured tungsten by introducing secondary-phase nanoparticles into the matrix. *Int J Refract Metals Hard Mater* 2019; 79: 158–163.
56. Hu Z, Zhao Y, Guan K, et al. Pure tungsten and oxide dispersion strengthened tungsten manufactured by selective laser melting: microstructure and cracking mechanism. *Addit Manuf* 2020; 36: 101579.
57. Xue J, Feng Z, Tang J, et al. Selective laser melting additive manufacturing of tungsten with niobium alloying: microstructure and suppression mechanism of microcracks. *J Alloys Compd* 2021; 874: 159879.
58. Aguirre M V, Martín A, Pastor JY, et al. Mechanical behavior of W–Y2O3 and W–Ti alloys from 25 °C to 1000 °C. *Metall Mater Trans A* 2009; 40: 2283–2290.
59. Ren C, Fang ZZ, Koopman M, et al. Methods for improving ductility of tungsten: a review. *Int J Refract Metals Hard Mater* 2018; 75: 170–183.
60. Klopp WD, Witzke WR and Raffo PL. Mechanical properties of dilute tungsten–rhenium alloys. *Natl Aeronaut Space Admin* 1966; 3483: 1–36.
61. Aguirre MV, Martín A, Pastor JY, et al. Mechanical properties of Y2O3-doped W–Ti alloys. *J Nucl Mater* 2010;404: 203–209.
62. Liu R, Xie ZM, Hao T, et al. Fabricating high performance tungsten alloys through zirconium micro-alloying and nano-sized yttria dispersion strengthening. *J Nucl Mater* 2014; 451: 35–39.
63. Zhang DQ, Liu ZH, Cai QZ, et al. Influence of Ni content on microstructure of W–Ni alloy produced by selective laser melting. *Int J Refract Metals Hard Mater* 2014;45: 15–22.
64. Wang D, Wang Z, Li K, et al. Cracking in laser additively manufactured W: initiation mechanism and a suppression approach by alloying. *Mater Des* 2019; 162: 384–393.
65. Kaserer L, Braun J, Stajkovic J, et al. Fully dense and crack free molybdenum manufactured by selective laser melting through alloying with carbon. *Int J Refract Metals Hard Mater* 2019; 84: 105000.
66. Dring K, Bhagat R, Jackson M, et al. Direct electrochemical production of Ti–10W alloys from mixed oxide preform precursors. *J Alloys Compd* 2006; 419: 103–109.
67. Froes FH (Sam). Additive manufacturing of titanium components: an up-date. *Metal Powder Report* 2018; 73: 329–337.
68. Withers JC and Pickard SM. *Additive manufacturing to produce standard and custom alloy titanium*. Pittsburg, PA, USA: The Minerals, Metals & Materials Series, 2017; 81–89.
69. Rane K and Strano M. A comprehensive review of extrusion-based additive manufacturing processes for rapid production of metallic and ceramic parts. *Adv Manuf* 2019; 7: 155–173.
70. Tseng J-W, Liu C-Y, Yen Y-K, et al. Screw extrusion-based additive manufacturing of PEEK. *Mater Des* 2018; 140: 209–221.
71. Zhao Z, Liu R, Chen J, et al. Additive manufacturing of cemented carbide using analogous powder injection molding feedstock. *Int J Refract Metals Hard Mater* 2023; 111: 106095.
72. Ziaee M and Crane NB. Binder jetting: a review of process, materials, and methods. *Addit Manuf* 2019; 28: 781–801.
73. Hillig WB. Melt infiltration approach to ceramic matrix composites. *J Am Ceram Soc* 1988; 71: C-96–C-99.
74. Arnold JM, Cramer CL, Elliott AM, et al. Microstructure evolution during near-net-shape fabrication of NixAly-TiC cermets through binder jet additive manufacturing and pressureless melt infiltration. *Int J Refract Metals Hard Mater* 2019; 84: 104985.
75. Tang J-Y, Luo L-M, Liu Z, et al. Shape retention of cemented carbide prepared by co melt infiltration into un-sintered WC green parts made via BJ3DP. *Int J Refract Metals Hard Mater* 2022; 107: 105904.
76. Cramer CL, Wieber NR, Aguirre TG, et al. Shape retention and infiltration height in complex WC–Co parts made via binder jet of WC with subsequent Co melt infiltration. *Addit Manuf* 2019; 29: 100828.
77. Yang Y, Zhang C, Wang D, et al. Additive manufacturing of WC–Co hardmetals: a review. *Int J Adv Manuf Technol* 2020; 108: 1653–1673.
78. Cramer CL, Aguirre TG, Wieber NR, et al. Binder jet printed WC infiltrated with pre-made melt of WC and Co. *Int J Refract Metals Hard Mater* 2020; 87: 105137.
79. Bose A, Reidy JP, Tuncer N, et al. Processing of tungsten heavy alloy by extrusion-based additive manufacturing. *Int J Refract Metals Hard Mater* 2022; 75: 106021.
80. Bose A, Schuh CA, Tobia JC, et al. Traditional and additive manufacturing of a new tungsten heavy alloy alternative. *Int J Refract Metals Hard Mater* 2018; 73: 22–28.
81. Li W and Leu MC. Material extrusion based ceramic additive manufacturing. *Addit Manuf Process. ASM Int* 2020; 24: 97–111.

82. Hu Z, Liu Y, Wu J, et al. The simultaneous improvement of strength and ductility of the 93W–4.6Ni–2.4Fe prepared by additive manufacturing via optimizing sintering post-treatment. *Addit Manuf* 2021; 46: 102216.
83. Liu J, Shukui L, Xiaoqing Z, et al. Adiabatic shear banding in a tungsten heavy alloy processed by hot-hydrostatic extrusion and hot torsion. *Scr Mater* 2008; 59: 1271–1274.
84. Friedel T, Travitzky N, Niebling F, et al. Fabrication of polymer derived ceramic parts by selective laser curing. *J Eur Ceram Soc* 2005; 25: 193–197.
85. Kruth J-P, Levy G, Klocke F, et al. Consolidation phenomena in laser and powder-bed based layered manufacturing. *CIRP Ann* 2007; 56: 730–759.
86. Kumar S. Manufacturing of WC–Co moulds using SLS machine. *J Mater Process Technol* 2009; 209: 3840–3848.
87. Travitzky N. Processing of ceramic–metal composites. *Adv Appl Ceram* 2012; 111: 286–300.
88. Barnett B, Trexler M and Champagne V. Cold sprayed refractory metals for chrome reduction in gun barrel liners. *Int J Refract Metals Hard Mater* 2015; 53: 139–143.
89. Moridi A, Hassani-Gangaraj SM, Guagliano M, et al. Cold spray coating: review of material systems and future perspectives. *Surf Eng* 2014; 30: 369–395.
90. Karthikeyan J, Industries. Inc. Development of Oxidation Resistant Coatings on GRCop 84, Substrates by Cold Spray Process. 2023.
91. Paul T, Joshi R, Walde C, et al. Multi-scale elastic behavior of cold sprayed refractory metal from splat to bulk deposit by integrated experimental and modeling approach. *Mater Sci Eng A* 2022; 853: 143751.
92. Kumar S, Jyothirmayi A, Wasekar N, et al. Influence of annealing on mechanical and electrochemical properties of cold sprayed niobium coatings. *Surf Coat Technol* 2016; 296: 124–135.
93. Kumar S, Ramakrishna M, Chavan NM, et al. Correlation of splat state with deposition characteristics of cold sprayed niobium coatings. *Acta Mater* 2017; 130: 177–195.
94. Ulianitsky VYu, Batraev IS, Shtertser AA, et al. Detonation spraying behaviour of refractory metals: case studies for Mo and Ta-based powders. *Adv Powder Technol* 2018; 29: 1859–1864.
95. Brodmann FJ. Cold spray process parameters: powders. *The Cold Spray Mater Depos Process* 2007; 1: 105–116.
96. Hassani-Gangaraj M, Veysset D, Champagne VK, et al. Adiabatic shear instability is not necessary for adhesion in cold spray. *Acta Mater* 2018; 158: 430–439.
97. He L, Veysset D, Nault IM, et al. Impact and bonding behavior of core–shell powder particles. *Surf Coat Technol* 2022; 441: 128591.
98. Hassani M, Veysset D, Sun Y, et al. Microparticle impact-bonding modes for mismatched metals: from Co-deformation to splatting and penetration. *Acta Mater* 2020; 199: 480–494.
99. Wang Q, Birbilis N and Zhang M-X. Interfacial structure between particles in an aluminum deposit produced by cold spray. *Mater Lett* 2011; 65: 1576–1578.
100. ASM International Handbook Committee. *Properties and selection: non ferrous alloys and special purpose materials*. 10th ed. USA: ASM International, 1990.
101. Zhou L, Chen J, Li C, et al. Microstructure tailoring to enhance strength and ductility in pure tantalum processed by selective laser melting. *Mater Sci Eng A* 2020; 785: 139352.
102. Jafarlou DM, Sousa BC, Gleason MA, et al. Solid-state additive manufacturing of tantalum using high-pressure cold gas-dynamic spray. *Addit Manuf* 2021; 47: 102243.
103. Hassani-Gangaraj SM, Moridi A and Guagliano M. Critical review of corrosion protection by cold spray coatings. *Surf Eng* 2015; 31: 803–815.
104. Kumar S and Rao AA. Influence of coating defects on the corrosion behavior of cold sprayed refractory metals. *Appl Surf Sci* 2017; 396: 760–773.
105. Koivuluoto H, Näkki J and Vuoristo P. Corrosion properties of cold-sprayed tantalum coatings. *J Therm Spray Technol* 2009; 18: 75–82.
106. Enneti RK, Prough KC, Wolfe TA, et al. Sintering of WC–12%Co processed by binder jet 3D printing (BJ3DP) technology. *Int J Refract Metals Hard Mater* 2018; 71: 28–35.
107. Yang G-J, Gao P-H, Li C-X, et al. Mechanical property and wear performance dependence on processing condition for cold-sprayed WC-(nanoWC-Co). *Appl Surf Sci* 2015; 332: 80–88.
108. Karthikeyan J. The advantages and disadvantages of the cold spray coating process. *The Cold Spray Mater Depos Process* 2007; 1: 62–71.
109. Celotto S, Pattison J, Ho JS, et al. The economics of the cold spray process. *The Cold Spray Mater Depos Process* 2007; 1: 72–101.
110. Mosallanejad MH, Niroumand B, Aversa A, et al. In-situ alloying in laser-based additive manufacturing processes: a critical review. *J Alloys Compd* 2021; 872: 159567.
111. Larimian T and Borkar T. Additive manufacturing of in situ metal matrix composites. In *Additive manufacturing of emerging materials*. Cham: Springer International Publishing; 2019; 1–28.
112. Enrique PD, Mahmoodkhani Y, Marzbanrad E, et al. In situ formation of metal matrix composites using binder jet additive manufacturing (3D printing). *Mater Lett* 2018; 232: 179–182.
113. Traxel KD and Bandyopadhyay A. Influence of in situ ceramic reinforcement towards tailoring titanium matrix composites using laser-based additive manufacturing. *Addit Manuf* 2020; 31: 101004.
114. Dadbakhsh S, Mertens R, Hao L, et al. Selective laser melting to manufacture "in situ" metal matrix composites: a review. *Adv Eng Mater* 2019; 21: 1801244.
115. Zang X, Tai KY, Jian C, et al. Laser-induced tar-mediated sintering of metals and refractory carbides in air. *ACS Nano* 2020; 14: 10413–10420.
116. Peters AB, Zhang D, Brupbacher MC, et al. Isovolumetric synthesis of chromium carbide for selective laser reaction sintering (SLRS). *Int J Refract Metals Hard Mater* 2019; 83: 104967.
117. Peters AB, Zhang D, Hernandez A, et al. Selective laser sintering in reactive atmospheres: towards in-situ synthesis of net-shaped carbide and nitride ceramics. *Addit Manuf* 2021; 45: 102052.
118. Peters AB, Hernandez A, Zhang D, et al. A reaction synthesis approach to additively manufacture net-shape chromium carbide and non-oxide refractory ceramics. *Addit Manuf* 2020; 34: 101186.
119. Roehling TT, Shi R, Khairallah SA, et al. Controlling grain nucleation and morphology by laser beam shaping in metal additive manufacturing. *Mater Des* 2020; 195: 109071.
120. Wischeropp TM, Tarhini H and Emmelmann C. Influence of laser beam profile on the selective laser melting process of AlSi10Mg. *J Laser Appl* 2020; 32: 022059.
121. Roehling TT, Wu SSQ, Khairallah SA, et al. Modulating laser intensity profile ellipticity for microstructural control during metal additive manufacturing. *Acta Mater* 2017; 128: 197–206.

122. Cloots M, Uggowitzer PJ and Wegener K. Investigations on the microstructure and crack formation of IN738LC samples processed by selective laser melting using Gaussian and doughnut profiles. *Mater Des* 2016; 89: 770–784.
123. Zhirnov Iv, Podrabinnik PA, Okunkova AA, et al. Laser beam profiling: experimental study of its influence on single-track formation by selective laser melting. *Mech Ind* 2015; 16: 709.
124. Ayoola WA, Suder WJ and Williams SW. Parameters controlling weld bead profile in conduction laser welding. *J Mater Process Technol* 2017; 249: 522–530.
125. Tumkur TU, Guss G, Roehling JD, et al. Metal additive manufacturing using complex beam shaping. *Proc CIRP* 2022; 111: 71–74.
126. Shi R, Khairallah SA, Roehling TT, et al. Microstructural control in metal laser powder bed fusion additive manufacturing using laser beam shaping strategy. *Acta Mater* 2020; 184: 284–305.
127. Tumkur TU, Voisin T, Shi R, et al. Nondiffractive beam shaping for enhanced optothermal control in metal additive manufacturing. *Sci Adv* 2021; 111: 71–74.
128. Rinne JS, Nothdurft S, Hermsdorf J, et al. Advantages of adjustable intensity profiles for laser beam welding of steel copper dissimilar joints. *Proc CIRP* 2020; 94: 661–665.
129. Feuchtenbeiner S, Hesse T, Speker N, et al. Beam shaping BrightLine weld: latest application results. In: Kaierle S and Heinemann SW (eds) *High-power laser materials processing: applications, diagnostics, and systems VIII*. San Francisco, CA, USA: SPIE; 2019, p. 31.
130. Victor B, Ream S and Walters CT. Custom beam shaping for high-power fiber laser welding. In International Congress on Applications of Lasers & Electro-Optics. Laser Institute of America; 2008. 1301.
131. Hansen KS, Kristiansen M and Olsen FO. Beam shaping to control of weldpool size in width and depth. *Phys Procedia* 2014; 56: 467–476.
132. Sanchez S, Hyde CJ, Ashcroft IA, et al. Multi-laser scan strategies for enhancing creep performance in LPBF. *Addit Manuf* 2021; 41: 101948.
133. Masoomi M, Thompson SM and Shamsaei N. Quality part production via multi-laser additive manufacturing. *Manuf Lett* 2017; 13: 15–20.
134. He C, Ramani KS and Okwudire CE. An intelligent scanning strategy (SmartScan) for improved part quality in multi-laser PBF additive manufacturing. *Addit Manuf* 2023; 64: 103427.
135. Yuan D, Sun X, Sun L, et al. Improvement of the grain structure and mechanical properties of austenitic stainless steel fabricated by laser and wire additive manufacturing assisted with ultrasonic vibration. *Mater Sci Eng A* 2021; 813: 141177.
136. Hu Y, Ning F, Cong W, et al. Ultrasonic vibration-assisted laser engineering net shaping of ZrO_2–Al_2O_3 bulk parts: effects on crack suppression, microstructure, and mechanical properties. *Ceram Int* 2018; 44: 2752–2760.
137. Li Y, Zhang D, Wang H, et al. Fabrication of a TiC-Ti matrix composite coating using ultrasonic vibration-assisted laser directed energy deposition: the effects of ultrasonic vibration and TiC content. *Metals (Basel)* 2021; 11: 693.
138. Ward AA, Zhang Y and Cordero ZC. Junction growth in ultrasonic spot welding and ultrasonic additive manufacturing. *Acta Mater* 2018; 158: 393–406.
139. Cong W and Ning F. A fundamental investigation on ultrasonic vibration-assisted laser engineered net shaping of stainless steel. *Int J Mach Tools Manuf* 2017; 121: 61–69.
140. Wang H, Hu Y, Ning F, et al. Ultrasonic vibration-assisted laser engineered net shaping of inconel 718 parts: effects of ultrasonic frequency on microstructural and mechanical properties. *J Mater Process Technol* 2020; 276: 116395.
141. Ning F and Cong W. Ultrasonic vibration-assisted (UV-A) manufacturing processes: state of the art and future perspectives. *J Manuf Process* 2020; 51: 174–190.
142. Zhu L, Yang Z, Xin B, et al. Microstructure and mechanical properties of parts formed by ultrasonic vibration-assisted laser cladding of inconel 718. *Surf Coat Technol* 2021; 410: 126964.
143. Chen W, Chen Y, Zhang T, et al. Effect of ultrasonic vibration and interpass temperature on microstructure and mechanical properties of Cu–8Al–2Ni–2Fe–2Mn alloy fabricated by wire arc additive manufacturing. *Metals (Basel)* 2020; 10: 215.
144. Todaro CJ, Easton MA, Qiu D, et al. Grain refinement of stainless steel in ultrasound-assisted additive manufacturing. *Addit Manuf* 2021; 37: 101632.
145. Gorunov AI. Additive manufacturing of Ti6Al4V parts using ultrasonic assisted direct energy deposition. *J Manuf Process* 2020; 59: 545–556.
146. Ji F, Qin X, Hu Z, et al. Influence of ultrasonic vibration on molten pool behavior and deposition layer forming morphology for wire and arc additive manufacturing. *Int Commun Heat Mass Transf* 2022; 130: 105789.
147. Li Y, Zhang D and Cong W. Ultrasonic vibration-assisted laser directed energy deposition of B4C-Ti composite: effect of laser power and ultrasonic vibration. In *Volume 2: Manufacturing processes; manufacturing systems; nano/micro/meso manufacturing; quality and reliability*. *American Society of Mechanical Engineers*; 2021.
148. Ning F, Hu Y, Liu Z, et al. Ultrasonic vibration-assisted laser engineered net shaping of inconel 718 parts: a feasibility study. *Proc Manuf* 2017; 10: 771–778.
149. Dai W-L. Effects of high-intensity ultrasonic-wave emission on the weldability of aluminum alloy 7075-T6. *Mater Lett* 2003; 57: 2447–2454.
150. Wang J, Sun Q, Wu L, et al. Effect of ultrasonic vibration on microstructural evolution and mechanical properties of underwater wet welding joint. *J Mater Process Technol* 2017; 246: 185–197.
151. Zhou S, Ma G, Dongjiang W, et al. Ultrasonic vibration assisted laser welding of nickel-based alloy and austenite stainless steel. *J Manuf Process* 2018; 31: 759–767.
152. Chen Q, Lin S, Yang C, et al. Grain fragmentation in ultrasonic-assisted TIG weld of pure aluminum. *Ultrason Sonochem* 2017; 39: 403–413.
153. Feng X, Zhao F, Jia H, et al. Numerical simulation of non-dendritic structure formation in Mg–Al alloy solidified with ultrasonic field. *Ultrason Sonochem* 2018; 40: 113–119.
154. Tian Y, Shen J, Hu S, et al. Effects of ultrasonic vibration in the CMT process on welded joints of Al alloy. *J Mater Process Technol* 2018; 259: 282–291.
155. Yuan T, Kou S and Luo Z. Grain refining by ultrasonic stirring of the weld pool. *Acta Mater* 2016; 106: 144–154.
156. Zhang X, Kang J, Wang S, et al. The effect of ultrasonic processing on solidification microstructure and heat transfer in stainless steel melt. *Ultrason Sonochem* 2015; 27: 307–315.
157. Zhao Y, Wu M, Hou J, et al. Microstructure and high temperature properties of laser cladded WTaNbMo refractory high entropy alloy coating assisted with ultrasound vibration. *J Alloys Compd* 2022; 920: 165888.

158. Nomura S, Murakami K and Kawada M. Effects of turbulence by ultrasonic vibration on fluid flow in a rectangular channel. *Jpn J Appl Phys* 2002; 41: 6601.
159. Todaro CJ, Easton MA, Qiu D, et al. Grain structure control during metal 3D printing by high-intensity ultrasound. *Nat Commun* 2020; 11: 142.
160. Ono K. A comprehensive report on ultrasonic attenuation of engineering materials, including metals, ceramics, polymers, fiber-reinforced composites, wood, and rocks. *Appl Sci* 2020; 10: 2230.
161. Li R, Ni Q-Q, Xia H, et al. Analysis of individual attenuation components of ultrasonic waves in composite material considering frequency dependence. *Compos B Eng* 2018; 140: 232–240.
162. Upadhye V and Agashe S. Effect of temperature and pressure variations on the resonant frequency of piezoelectric material. *Meas Control* 2016; 49: 286–292.
163. Wellendorf A, von Damnitz L, Nuri AW, et al. Determination of the temperature-dependent resonance behavior of ultrasonic transducers using the finite-element method. *J Vibr Eng Technol* 2023: 1–14.